Designing alumina-zirconia composites by DLP-based stereolithography: Microstructural tailoring and mechanical performances

Designing alumina-zirconia composites by DLP-based stereolithography: microstructural tailoring and mechanical performances

Bartolomeo Coppola[1,+,*], Tanguy Lacondemine[2,+], Caroline Tardivat[2], Laura Montanaro[1] and Paola Palmero[1]

[1] Politecnico di Torino, Department of Applied Science and Technology, INSTM R.U. Lince Laboratory, Corso Duca Degli Abruzzi, 24, Italy

[2] LSFC Laboratoire de Synthèse et Fonctionnalisation des céramiques UMR 3080 CNRS / Saint-Gobain CREE, Saint-Gobain Research Provence, 550 avenue Alphonse Jauffret, Cavaillon, France

[+] These authors equally contributed to this work

[*] Corresponding author: bartolomeo.coppola@polito.it

Abstract

Digital Light Processing (DLP) is attracting high interest thanks to the possibility to prepare dense or complex ceramic parts starting from a photosensitive ceramic slurry. ZrO_2 and Al_2O_3 are the most studied ceramic materials for DLP, while few studies deal with their composites in spite their wide range of applications. In this work, three alumina-zirconia composites (at 15, 50 and 85vol% of ZrO_2) were prepared by mixing ready-to-use ZrO_2 and Al_2O_3 slurries. The mechanical and physical properties of the composites prepared via DLP technique were investigated and compared to those of neat alumina and zirconia materials used as a reference. For each composite, the sintering temperature was optimized on the ground of final density and microstructural development, with the aim to achieve a target density (i.e. $\rho > 98.5\%TD$), while

keeping a fine microstructure. The composites were characterized by quite homogeneous microstructures, with a good distribution of the two phases, in line with the materials prepared by conventional techniques. Flexural strength, elastic modulus and Vickers hardness of fabricated alumina-zirconia composites ranged between 415-843 MPa, 188-318 GPa and 15-21 GPa, respectively. These results show that the well-known microstructure-properties relationship, which dominates the conventionally fabricated materials, also plays an important role in stereolithography processed samples. In fact, once optimized the fired densities and the microstructures, the 3D-printed alumina-zirconia composites reached mechanical properties higher than almost all previous investigations for the same composites fabricated by stereolithography, and in most cases even higher than those of conventional composites of analogous compositions.

Keywords: Stereolithography, Digital Light Processing; 3D printing; alumina-zirconia composites; Microstructure; Mechanical properties

1. Introduction

Additive Manufacturing (AM) technologies, also referred as 3D printing, are changing the way to fabricate parts for several class of materials: polymers, metals and, more recently, ceramics [1-8]. The introduction of 3D printing technologies for the manufacturing of technical ceramics allows to overcome most issues of conventional ceramic shaping techniques. In fact, such conventional techniques cannot be used for the direct fabrication of parts with complex shapes (like internal holes, sharp corners, etc.) and great accuracy, but always require a post-production machining, such as cutting and surface polishing [9-11]. The 3D printing technologies of technical ceramics can be divided into three categories, considering raw-material form prior to printing: slurry-based, powder-based and bulk solid-based methods [6-8]. Among the slurry-

based methods, stereolithography (SL) is particularly advantageous in terms of resolution, accuracy and surface finishing.

Recently, SL was successfully used to process technical ceramics like alumina and zirconia, as attested by the numerous scientific publications [12-41]. On the opposite, few studies relate to alumina-zirconia composites [42-48], which are currently considered the golden standard for several mechanical and biomedical applications. These composites, in fact, join the excellent hardness and wear resistance of α-alumina with the very high bending strength and fracture toughness of yttria-stabilized tetragonal zirconia polycrystals (3Y-TZP), finding applications as cutting tools, bearing parts, biomaterials for orthopedic and dental implants, thermal and corrosion-resistant coatings [49-54]. In relation to the zirconia amount, they are known as Zirconia Toughened Alumina (ZTA) composites, where a relatively low amount (5-20wt%) of ZrO_2 provides toughness and reliability, or Alumina Toughened Zirconia (ATZ), in which larger alumina particles embedded in a fine zirconia matrix provide toughness, hardness and strength. When conventional manufacturing is used, the careful control of the processing parameters and the tailoring of the sintered microstructures and compositions are the keys to achieve high physical and mechanical properties. In fact, fully dense and fine microstructures, with an even distribution of the two phases in the composites, are necessary to achieve high strength, hardness and resistance to crack propagation [55,56].

Concerning the development of ZTA composites by SL, Xing et al. [43] investigated the influence of the particle size distribution (PSD) on the viscosity of UV-curable pastes based on alumina and zirconia particles. According to their model, an ideal paste with relatively good fluidity has to be prepared by ceramic powders with bimodal PSD, uniformly dispersed in the photosensitive resins. Accordingly, the authors determined an optimal viscosity of 30000 mPa s at 30 s^{-1} shear rate with slurries at 47vol% solid loading, with 15vol% fine zirconia particles, and the remaining fraction composed by 30vol% fine alumina and 70vol% large alumina particles. The composite showed a very high density (up to 99.4%) and good mechanical properties (flexural strength and hardness equal to 535 MPa and 17.8 GPa, respectively). Wu et

al. [46] developed a single ZTA composition, at 4:1 alumina:zirconia weight ratio, and investigated the role of sintering temperature on fired density, hardness and fracture toughness. They found that ZTA density increased with the sintering temperature up to 1600 °C, while it dropped after a further temperature increase (i.e. 1650 °C). The maximum Vickers hardness (17.6 GPa) and maximum fracture toughness (5.2 $MPa \cdot m^{1/2}$) were determined after sintering at 1550 °C and at 1650 °C, respectively. Similarly, Liu et al. [42] investigated the influence of sintering temperature and holding time on the hardness and fracture toughness of ZTA, containing 15vol% ZrO_2. The authors determined density, hardness and fracture toughness as 3.75 g/cm^3, 14.1 GPa and 4.05 $MPa \cdot m^{1/2}$, respectively, at the maximum sintering temperature of 1500 °C for 1h. Similarly, Zheng et al. [47] developed a single ZTA composite, at 3:1 alumina:zirconia weight ratio, sintered at 1600°C. Density and mechanical properties (hardness, fracture toughness and bending strength) were significantly higher than those of pure alumina sintered under the same conditions.

Considering ATZ composites, Schwarzer et al. [44] developed printable slurries by using a commercial ATZ powder, and successfully printed complex lattice structures. However, they obtained a discrepancy (15 to 30%) between theoretical and measured dimensions of the cavities due to samples overcuring and suboptimal cleaning. Borlaf et al. [45] developed zirconia and ATZ (at 20wt% Al_2O_3) slurries by one or two-step procedures, followed by sintering at 1450 °C for 2h, reaching a high fired density (~ 99%) and flexural strength (~800 MPa).

Such previous investigations attest the strong interest of the scientific community towards the development of alumina-zirconia ceramics by digital-light printing process, but also underline the lack of a comprehensive investigation, particularly in relation to the role of the composition (i.e., alumina/zirconia ratio) on the microstructural development and final mechanical properties. Here, a simple approach to prepare alumina-zirconia slurries at different relative ratios was employed, by mixing ready-to-use alumina and zirconia commercial slurries. Composite samples, at three compositions (at 15, 50 and 85vol% ZrO_2), sintered at different

temperatures in the range 1500 – 1600°C, were optimized on the ground of fired density and microstructural development. Mechanical properties (hardness, elastic modulus and bending strength) were determined and compared to those of reference alumina and zirconia samples but also to literature data, discussing the results on the ground of composites' peculiar microstructural and compositional features.

2. Material and methods

2.1. Materials

Two commercial slurries (purchased from Admatec Europe BV, The Netherlands) made of α-alumina and 3mol% yttria-tetragonal zirconia polycrystal (3Y-TZP) (AdmaPrint A130 and AdmaPrint Z130, respectively) were used. In order to investigate the features of the raw materials, such commercial slurries were calcined, in order to remove the monomer, and then submitted to FE-SEM characterization. As we can observe from the FE-SEM micrographs (Figure 1), the starting alumina powder was composed by ultrafine grains (of about 200 nm in size), even if some larger grains can be observed as well (white arrows in Figure 1a). Such observation suggest a bimodal size distribution of the alumina particles within the slurry. Moreover, the powder was submitted to EDX analysis (data not reported), which confirmed that the powder was composed by pure alumina, and no magnesium traces (generally used as grain growth inhibitor) were found. As-received zirconia slurry was submitted to the same calcination step, and the resulting powder submitted to FE-SEM observations too (Figure 1b). Also in this case we observed that the starting powder was composed by ultrafine grains (lower that 200 nm), with a narrower and more homogenous particle distribution as respect to alumina. Light curing slurries contain a photoreactive resin with approx. 50vol% ceramic powder loading. Alumina-zirconia composites, with Al_2O_3/ZrO_2 volume fractions of 85/15, 50/50 and 15/85, were obtained by mixing the two original slurries, already optimized for printing. To mix suitable slurries amounts for obtaining the desired Al_2O_3/ZrO_2 volume fractions, the actual solid loading of the ceramic particles into the two polymer resins was determined. To this aim, DTA-

TG analyses (Netzsch STA 409, Germany) were performed up to 1000 °C, under static air, providing an Al_2O_3 content of 70.8wt% and a ZrO_2 content of 74.6wt% in the original slurries. Samples are labelled in the following way: A for alumina, Z for zirconia, AZ15, AZ50 and AZ85 for the composites at 15, 50 and 85vol% ZrO_2, respectively.

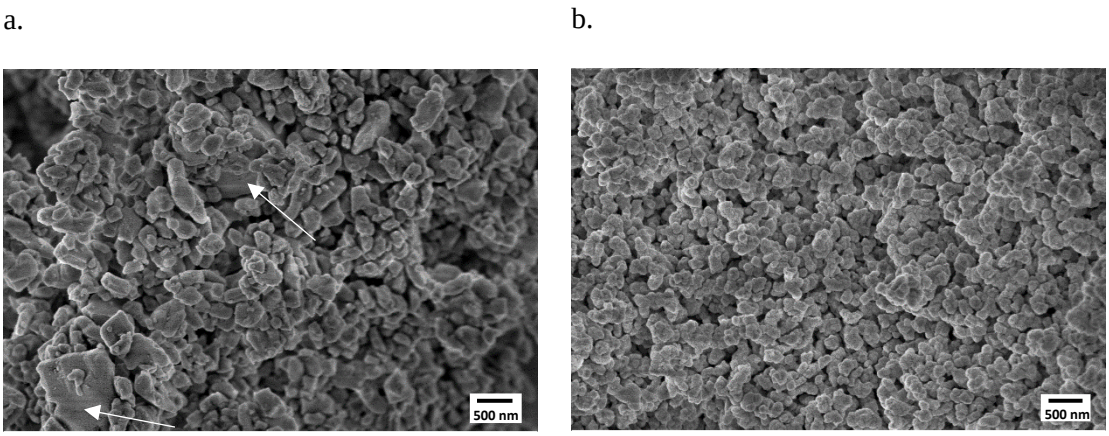

Figure 1: FE-SEM micrographs of a) alumina and b) zirconia powder deriving from commercial slurries calcination (white arrows indicate alumina larger particles)

2.2. Digital Light Processing (DLP) and post-processing

Prismatic samples (32 x 3 x 4 mm, length x width x height) were designed using AutoCAD software. A linear shrinkage ratio (of approx. 20% in x and y direction; approx. 30% in z) must be taken into account during design to obtain final dimensions after sintering. Parts were printed using a DLP-based additive manufacturing device ADMAFLEX 130 (ADMATEC Europe BV, The Netherlands), in which the ceramic slurry is stored in a reservoir and the transport foil combined with a doctor blade allow to deposit a layer of constant thickness of 125 μm [57]. Samples were printed onto an aluminum plate using a layer thickness of 30 μm. A delay of 40 s before exposure was needed to let air bubbles to flow out from the slurry. An exposure time of 3 s and power led of 450‰ were set so that the curing depth was equivalent to approx. 2 layers' thickness, preventing delamination.

After printing, the samples were immersed in deionized water at approx. 40 °C for 24 h to remove extra-slurry. Then, the samples were oven dried at 70 °C for 6 hours, and submitted to

thermal debinding performed in an electric furnace (Carbolite 1200, Carbolite Gero GmbH) under air atmosphere, according to the following thermal cycle (Figure 2):

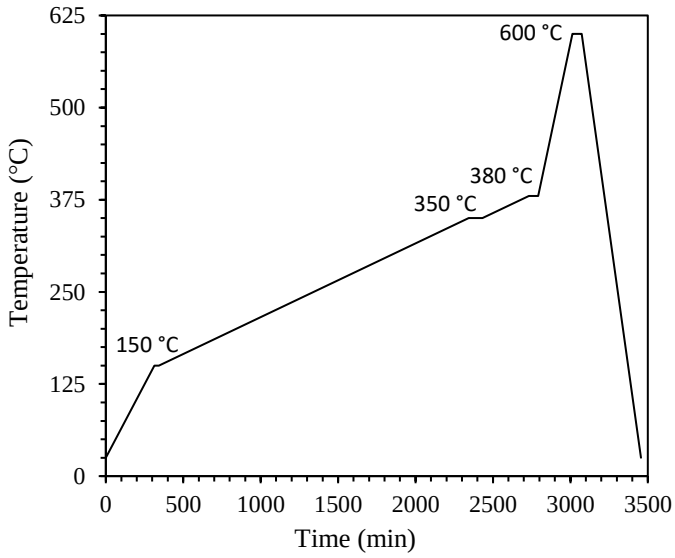

Figure 2: Thermal debinding cycle

Neat alumina and zirconia samples were sintered at 1625 °C/1h and 1500 °C/1h, respectively, on the ground of previous literature data on SLA-processed materials [24,35]. Both materials reached a relative density > 98 % TD, considering as reference a theoretical density of 3.98 g/cm^3 for alumina and 6.05 g/cm^3 for yttria-stabilized zirconia (3Y-TZP). Alumina-zirconia composites were sintered at different temperatures ranging between 1500 and 1600 °C, and the optimal sintering temperature of each composition was selected on the ground of systematic study of either fired density or microstructural development. While the maximum sintering temperature was optimized for each composition, the thermal cycles were similar, with a first heating step at 2 °C/min to 600 °C, a second heating step at 1 °C/min to 1000 °C for 1 h, and third heating step at 1 °C/min to the maximum sintering temperature, with 1 h dwell.

2.2 Characterization

The density of the ceramic parts, ρ (g/cm^3), was determined by buoyancy method, following Archimedes' principle (Density Determination Kit, Sartorius YDK01). The dimensions of the green and sintered samples were measured using a micrometer caliper to calculate the linear

shrinkage ratios in the three directions (x: length, y: width, z: height). The microstructures of the green and sintered bodies were characterized by means of a FE-SEM (Zeiss Supra-40, Oberkochen, Germany) equipped with an Oxford Energy Dispersive X-ray detector. The surfaces of the sintered samples were polished down to 1 μm with diamond paste and thermal etched at 100 °C below sintering temperature (heating rate of 10 °C/min, with 10 min dwell). The grain size of both Al_2O_3 and ZrO_2 phases were determined by image analysis, by using the Scandium Soft imaging system software; between 200 and 500 grains were measured for each phase, composite composition and sintering temperature.

The phase composition was determined by X-ray diffraction in Bragg-Brentano configuration (X'Pert Powder DY 3539), in the 5-70° 2θ range. Phases were identified by JCPD file n. 46-1212 for Al_2O_3, 01-083-0113 for tetragonal Y-stabilized ZrO_2, and 81-1314 for monoclinic ZrO_2. The intensities of the monoclinic (-111) and (111) peaks and the (101) tetragonal peak were integrated to calculate the volume of monoclinic zirconia in the composites, according to the Garvie Nicholson method.

Samples densified at their optimized sintering conditions (selected on the ground of fired density and microstructure) were submitted to mechanical testing. Hardness was measured by means of Vickers indentation (MicroMet 6000 Series Buehler) after surface polishing down to 1 μm. A series of 10 indentations were performed on each material with applied load ranging from 100 g_f for pure alumina to 500 g_f for pure zirconia and ATZ/ZTA composites, with a dwell of 15 s. The hardness was calculated from the applied load, previously selected to avoid cracks, and the two diagonals length, according to the standard equation [58].

Samples flexural strength was determined by 3 points bending tests using a Shimadzu AGSX traction/compression machine. Ten samples of dimensions 25 x 2 x 3 mm (L x W x H) were tested with a crosshead speed of 100 μm/s and a support span of 20 mm. The load was measured thanks to a 10 kN force sensor and the sample deflection, under the loading pin, was measured during testing thanks to a Linear Variable Differential Transformer (LVDT) sensor. The

Young's Modulus of the different materials was estimated from the linear slope of the load-displacement curves.

Crystalline phases identification was carried out by XRD analysis performed on polished surfaces of sintered samples using a Pan'Analytical X'Pert Pro instrument (Pan'Analytical, Almelo, The Netherlands) with CuKα radiation (0.154056 nm) in the 2θ range 20-65°.

3. Results & discussion

3.1. Density and microstructure

Figure 3 shows the cross section micrographs of an as-printed alumina sample after water debinding. In the lower magnification image (Figure 3a) it is possible to appreciate both the accuracy and precision of the printing process. In fact, considering that the imposed layer thickness was 30 μm, the actual layers range between 27 and 29 μm. No delamination among the layers was observed, highlighting the correct choice of the printing parameters and consequently of the curing depth [15]. By the same image, we can observe a good compactness of the 3D printed sample, free from large defects. Moreover, the as-printed microstructure was quite homogeneous, with ultra-fine alumina particles embedded in the residual polymer, as depicted in the higher magnification image (Figure 3b).

a. b.

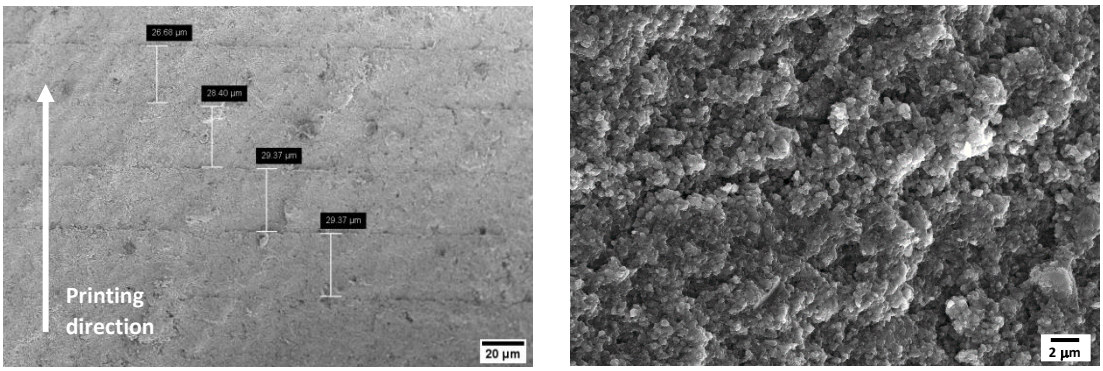

Figure 3: FE-SEM micrographs (cross section) of an as-printed and water-debinded alumina sample, at lower (a) and higher (b) magnifications

The sintered microstructures of neat alumina and zirconia samples are shown in Figure 4. At the selected sintering temperatures, both materials reached a high densification degree, precisely 98.5% for alumina and 99.1% for zirconia. Alumina showed a bimodal size distribution, made by fine grains (1- 2 microns in size) surrounded by abnormally grown grains, accompanied by pore entrapment within the coarsened grains [59]. The average size was 2.85 ± 2.13 μm, and the observed residual porosity was in line with the sintered alumina density. On the opposite, sintered zirconia showed an almost fully dense and completely homogeneous microstructure, with an average size of 0.35 ± 0.03 μm.

a. b.

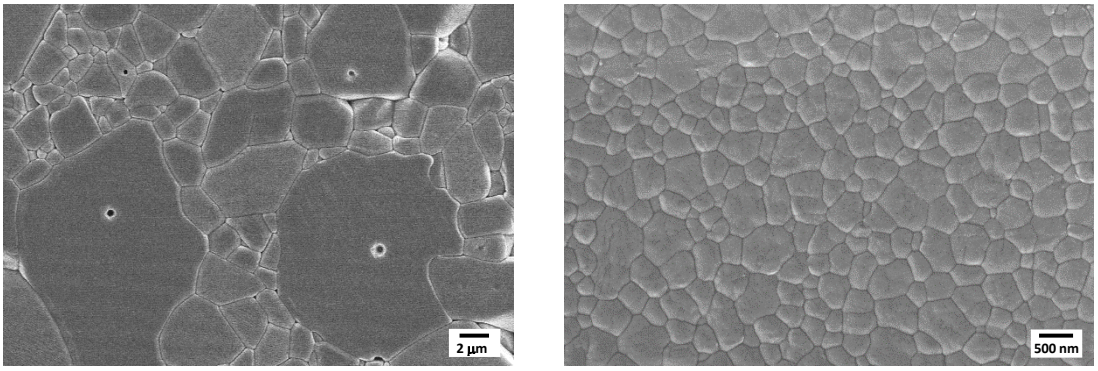

Figure 4: FE-SEM micrographs of sintered alumina (1650 °C/1h) and zirconia (1500 °C/1h) printed materials

Starting from the fired density and the observed microstructures of the pure materials, alumina-zirconia composites were sintered at different temperatures in the range 1500 °C-1600 °C. Figure 5(a) shows the fired density as a function of the sintering temperatures, showing an expected increase of the density with the sintering temperature, for all three composites. In addition, the higher the zirconia content, the lower the temperature needed to obtain a high relative density ($\rho \geq 98.5\%$ TD). In fact, while AZ85 achieved this target at all the investigated temperatures, AZ50 and AZ15 needed 1600 °C to reach the same final density. Finally, we can observe that at a fixed sintering temperature, a linear relationship between relative density and zirconia content exists, as depicted in Figure 5(b) for samples sintered at the intermediate temperature of 1550 °C (red circles). In the same figure, the relationship between density and

zirconia amount is also depicted at 1500 °C (black squares), in which the 100vol% ZrO_2 (sample Z) was also included, showing the same linear behavior.

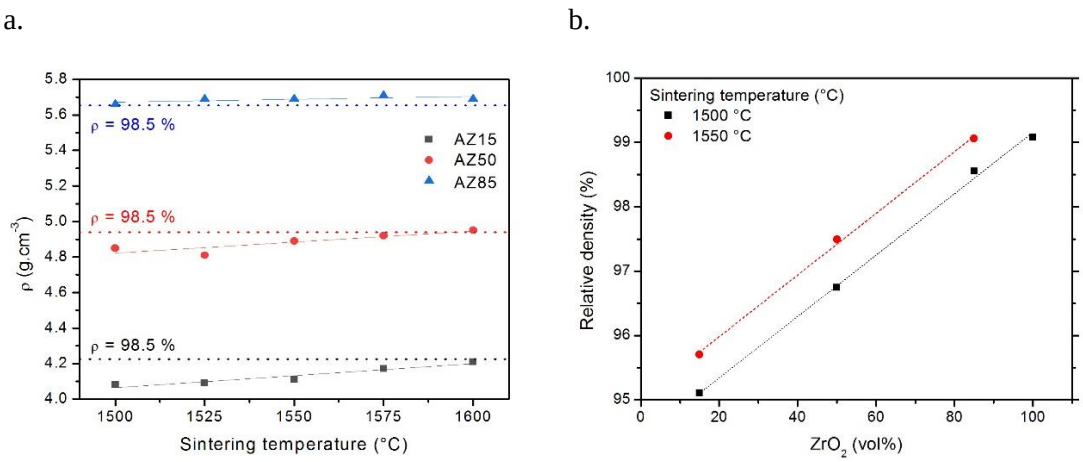

Figure 5: Density variation of alumina-zirconia composites, as a function of: a. the sintering temperature; b. the zirconia volume content at fixed temperatures (i.e. 1500 and 1550 °C)

FE-SEM observations were carried out to investigate the homogeneity of phases distribution in the composites. Image analyses were carried out as well, to observe the grain size evolution as a function of the sintering temperature. FE-SEM micrographs of the three composites, and related particle size distributions for both Al_2O_3 and ZrO_2 grains are depicted in Figure 6-8. As a general comment, we can observe a quite good distribution of the two phases into the composite materials. Zirconia grains showed a sub-micrometric average size, in all the three composites and at all the sintering temperatures. Alumina grains showed larger size distributions; however, even though some coarsened grains can be easily observed (see for instance the arrows in Figure 6b), abnormal grain growth was never observed in the composites. This observation confirms the important role played by the fine zirconia grains, evenly distributed in the alumina matrix, in limiting the matrix grain growth and particularly the abnormal growth phenomena. In AZ15 (Figure 6) some residual pores, mainly located at grain boundaries and intergranular positions, can be easily observed, in line with its mean fired density. In this composition, alumina and zirconia phases were characterized by a significantly different particle size distribution. Particularly, zirconia grains were smaller and characterized by a narrower size distribution as

respect to alumina. Zirconia grains were mainly located at alumina grain boundaries and triple or multiple junctions are visible, while in few cases ultrafine ZrO_2 grains were located inside the alumina particles.

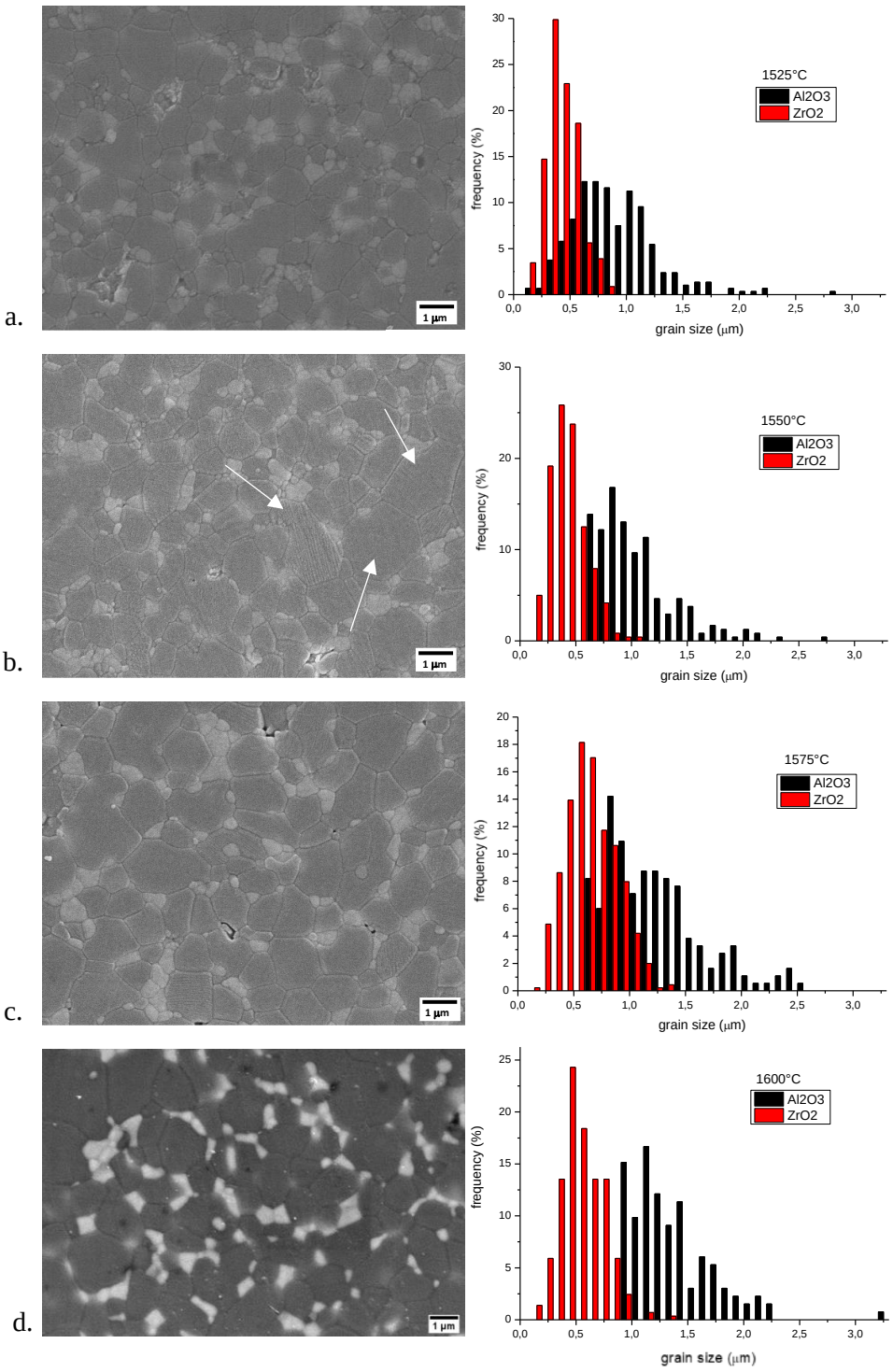

Figure 6: FE-SEM images of AZ15 composites and related grain size distributions, as a function of sintering temperature (a. 1525, b. 1550, c. 1575 and d. 1600 °C)

In addition, while the sintering temperature played a moderate role on zirconia grain growth, as similar distributions can be observed by moving from 1525 °C to 1600 °C, a progressive displacement of alumina grains towards higher size values can be observed.

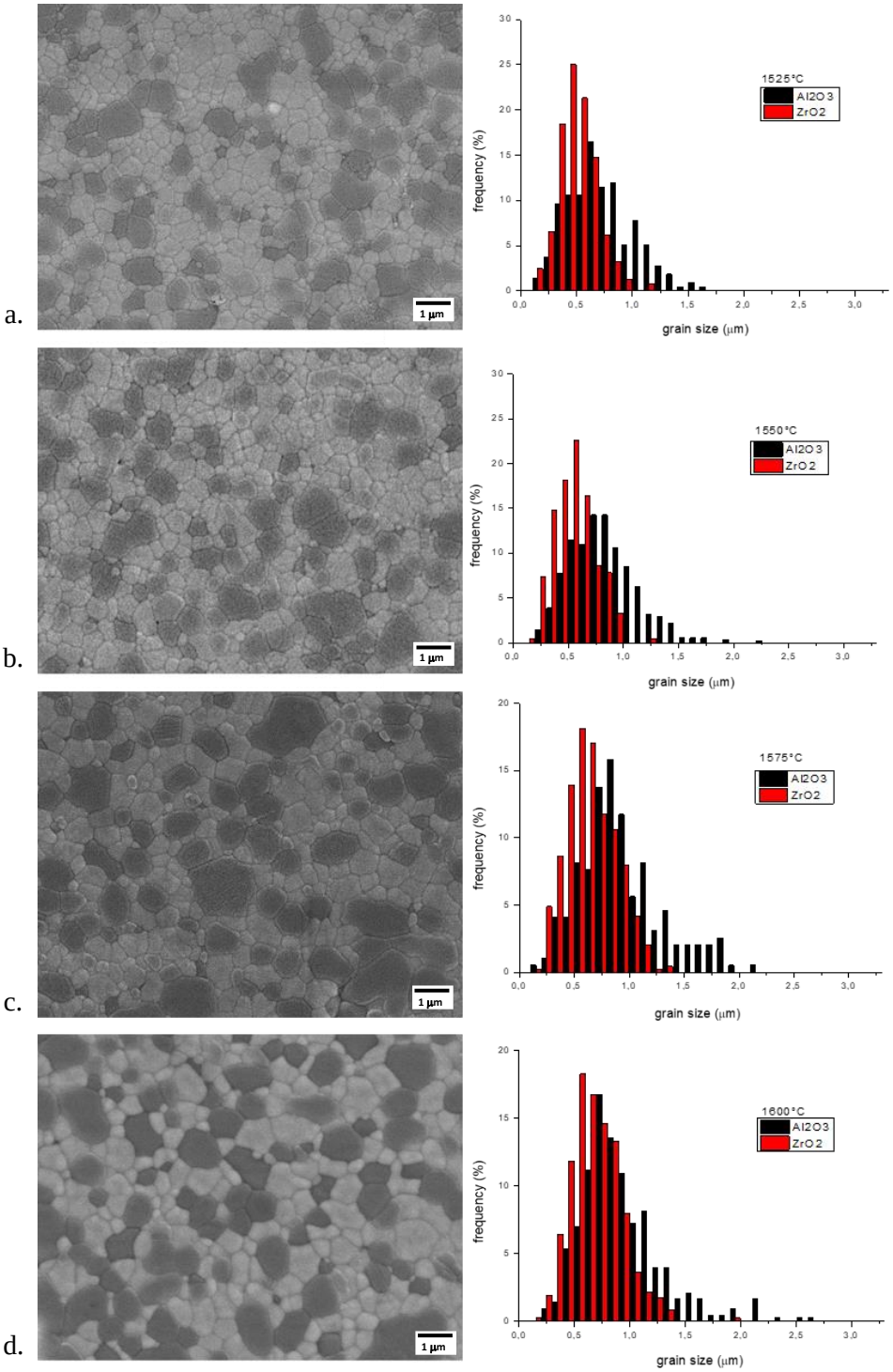

Figure 7: FE-SEM images of AZ50 composites and related grain size distributions, as a function of sintering temperature (a. 1525, b. 1550, c. 1575 and d. 1600 °C)

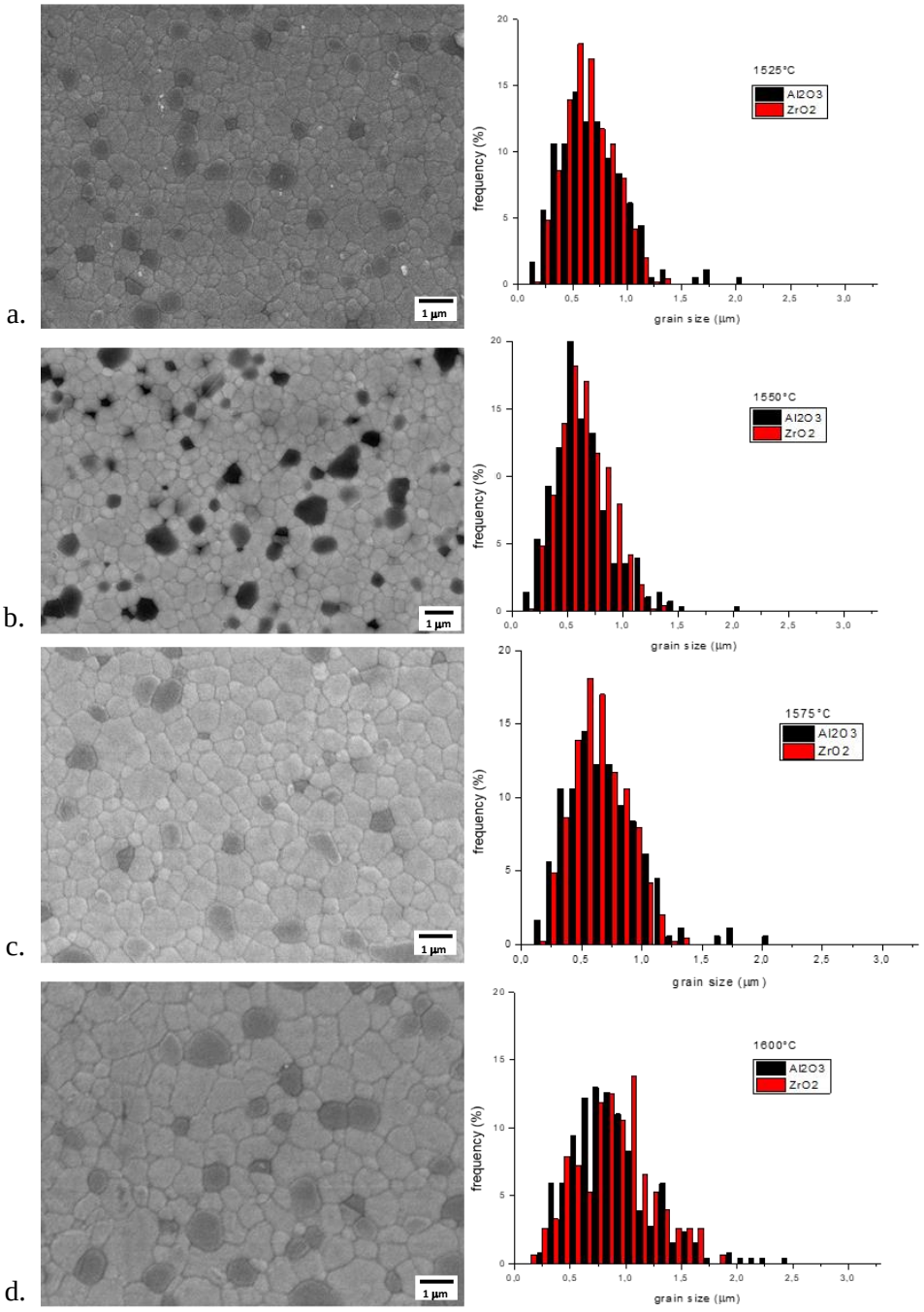

Figure 8: FE-SEM images of AZ85 composites and related grain size distributions, as a function of sintering temperature (a. 1525, b. 1550, c. 1575 and d. 1600 °C)

A completely different microstructure was observed in AZ50 (Figure 7), where the increase of the zirconia content induced a progressive refinement of the alumina phase and of the overall microstructures [60]. While in AZ15 the matrix refinement can be imputed to the pinning effect exerted by the fine ZrO_2 grains on the alumina grain boundaries, in AZ50 a typical duplex

microstructure made by two immiscible phases was obtained, where (mutual) grain growth retardation was due to the longer interdiffusion distance between grains of the same phase [61]. Such grain growth retardation mechanism was very effective, as evidenced by the fact that the alumina particle size distribution in AZ50 was displaced at significantly lower values than in AZ15. In addition, such duplex microstructure showed an increased stability in temperature compared to AZ15, as evidenced by the negligible growth observed for the alumina grains moving from 1525 °C to 1600 °C.

Finally, in AZ85 (Figure 8) isolated alumina grains were embedded in the zirconia immiscible phase, thus making even longer the atomic diffusion distances and further preventing alumina grain growth. As a result, alumina and zirconia particle size distribution were almost superimposable in this composite; the sintering temperature displayed a moderate effect moving from 1525 °C to 1550 °C, while the grain growth was more significant at the highest temperatures.

The effect of the sintering temperature on grain size is depicted in Figure 9. Once again we can observe the progressive decrease of the alumina particle size (and related standard deviation) by increasing the zirconia content. Moreover, a linear increase of the particles size with the sintering temperature, for both Al_2O_3 and ZrO_2 phases and in all three composites, can be stated. The slope of such linear trends depends on the composition: at low zirconia amount (AZ15), the slope of the alumina line is higher than zirconia one, and the opposite trend is observed in the specular composite (AZ85), while in AZ50 alumina and zirconia show almost parallel evolutions.

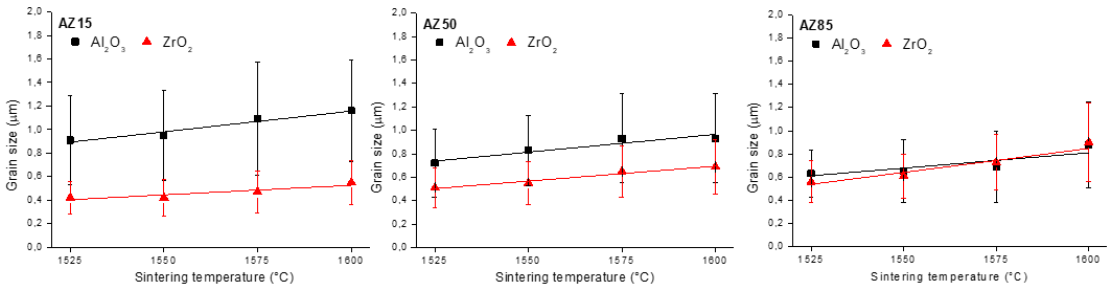

Figure 9: Alumina and zirconia grain size evolution as a function of the sintering temperature for AZ15, AZ50 and AZ85 composites

The correctness of the slurry mixing method to obtain composites with the three nominal Z/A volume ratios was demonstrated for the AZ50 composite by EDX analysis. Several spectra were acquired on large composite areas, providing a mean Zr/Al molar ratio of 0.642, close to the nominal value of 0.629, and which corresponds to 49.5vol% Al_2O_3/50.5vol% ZrO_2 composition, in a very good agreement with the expected volume fractions.

On the ground of sintered density, microstructural observations and size evolution, the best sintering conditions for each composite were selected, and samples produced under those conditions were submitted to mechanical testing, as reported later on. Specifically, AZ15 was sintered at 1600°C for 1h, as at this temperature the material density (98.1%) approached the target one, without excessive microstructural coarsening. The same maximum sintering temperature was selected for AZ50, once again due to the high density reached (98.8%) and the final tailored microstructure. For AZ85, it was possible to decrease the maximum sintering temperature at 1550 °C, where the high fired density (99.1%) was accompanied by fine and narrow particle size distribution. In Table 1, the fired density and the mean grain size of pure alumina and zirconia ceramics (used as a reference) and of the composite materials submitted to mechanical testing are collected.

Table 1: Density and mean alumina and zirconia grain size of samples submitted to mechanical testing

Material		A	AZ15	AZ50	AZ85	Z
Max. sintering temperature (°C)		1625	1600	1600	1550	1500
Sintered density (g/cm^3)		3.92 ± 0.02	4.22 ± 0.03	4.96 ± 0.02	5.69 ± 0.01	5.99 ± 0.03
Mean grain size (µm)	Al_2O_3	2.85 ± 2.13	1.16 ± 0.43	0.93 ± 0.38	0.65 ± 0.27	-
	ZrO_2	-	0.55 ± 0.19	0.69 ± 0.23	0.61 ± 0.19	0.35 ± 0.03

Finally, crystalline phases present in the sintered materials were identified using XRD analysis and the patterns are reported in Figure 10. As expected, ATZ and ZTA composites present both alumina and zirconia characteristic peaks, according to neat A and Z samples. Very few amounts of monoclinic ZrO_2 are present only in Z and AZ85 samples (2.6% and 4.6%, respectively, according to Garvie Nicholson model [62]) while most of the zirconia is in the tetragonal phase, meaning that stress induced martensitic phase transformation (i.e. tetragonal to monoclinic) can occur in all composites.

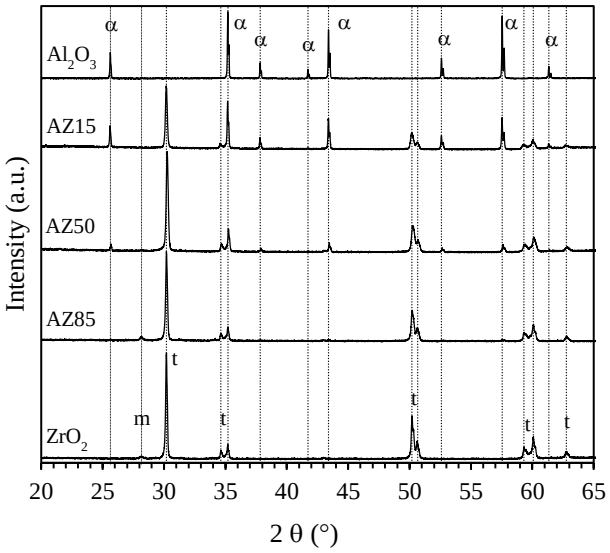

Figure 10: XRD patterns corresponding to Al_2O_3, AZ15, AZ50, AZ85 and ZrO_2 samples sintered at 1625 °C, 1600 °C, 1600 °C, 1550 °C and 1500 °C for 1h, respectively. m = monoclinic ZrO_2; t = tetragonal ZrO_2 and α = α-Al_2O_3

3.2. Mechanical properties

The results of the Vickers indentation test demonstrated that hardness is not dependent on the printing direction: similar values were in fact measured on surfaces perpendicular and parallel to the layers' orientation, in agreement with previous literature [14].

The evolution of the hardness as a function of zirconia content is shown in Figure 11, where the mean value is calculated over 10 measurements. A and Z samples show mean hardness values of 19.35 ± 1.08 and 12.73 ± 0.25 GPa, respectively, which are closed to conventionally shaped materials properties [52,63]. In the case of pure zirconia, the lowest average hardness value is also accompanied by the smallest standard deviation, which proves again the high degree of density and microstructural homogeneity of this printed material. These values are also comparable to reported hardness of 3D printed alumina [34] and zirconia [12] ceramics obtained by lithography-based manufacturing techniques. The composites showed hardness values in the range ~ 15 – 21 GPa, with an expected decrease by increasing the zirconia content. However, starting from the experimental values of alumina and zirconia reference samples, and by applying the rule of mixtures [64], the nominal hardness of the composites was calculated (empty symbols in Figure 11). All the experimental hardness values were higher than the nominal ones, and AZ15 reached a mean value (21.14 ± 1.64 GPa) even higher than monolithic alumina. Such behavior can be imputed to the significant microstructural refinement of the composites as respect to reference alumina, due to the well-known Hall-Petch relation [65]. The value reached by AZ15 is much higher than literature values for similar materials with equivalent density produced by stereolithography [46,48] or conventional processing (slip casting) [66]. The AZ50 and AZ85 composites were characterized by mean hardness of 17.21 ± 0.93 and 15.36 ± 0.77 GPa, respectively. Due to the high density and the fine and homogeneous microstructure, their hardness is larger than those of identical composites manufactured by isostatic or uniaxial pressing [67,68].

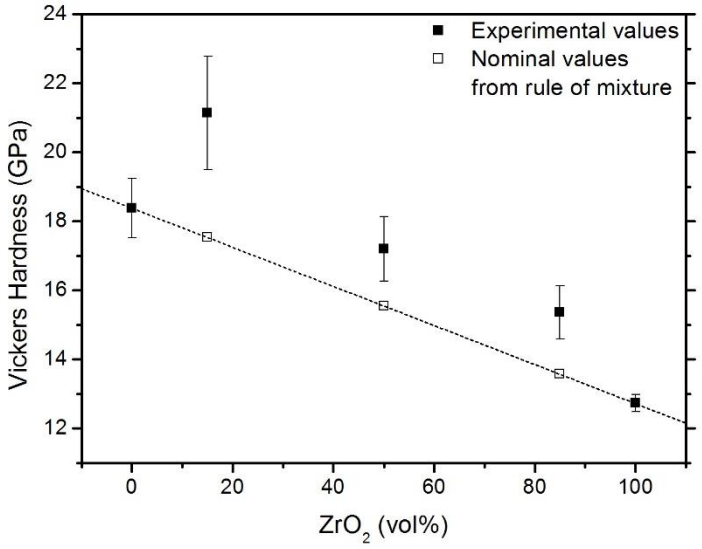

Figure 11: Vickers hardness as a function of zirconia content. Full symbols: experimental values; empty symbols: nominal values by the rule of mixtures

The three-point bending tests were performed on 10 samples for each material, and results depicted in Figure 12 (a). The samples were tested straight after sintering, without any additional polishing steps, in such a way that the measured bending strengths of the 3D printed alumina-zirconia ceramics are process-dependent and sensitive to defects generated during manufacturing. In addition, their load-displacement curves were perfectly linear, so that the calculated slopes allowed to determine the Young's modulus, as shown in Figure 12 (b). The alumina samples exhibited a bending strength of 415 ± 24 MPa and Young's modulus of ~ 334 ± 16 GPa. These values are within the range of conventional dense alumina properties [63,69]. The high mean strength value and low standard deviation compared to previously reported dense alumina obtained by stereolithography (ρ = 98.2 %, σ = 363.7 ± 74.6 MPa [70]) are evidences of the samples consistency and low defect rate at the surfaces. A high bending strength of 693 ±87 MPa was reached for the AZ15 composite (E = 318 ± 15 GPa), that is more than 150 MPa greater than SLA manufactured zirconia toughened alumina (ZTA) with equivalent A/Z volume fractions (σ = 530.29 ± 29.57) [48]. The resulting bending strength for the AZ50 and AZ85 composites are 843 ± 67 MPa and 764 ± 136 MPa, with corresponding Young's Moduli of 268 ± 4 GPa and 213 ± 15 GPa, respectively. Analogous alumina

toughened zirconia, with 50 vol% and 15 vol% of alumina, were elaborated by isostatic pressing [67], but the strength was determined by biaxial bending and the comparison with the current study is therefore not straightforward. At last, the mean bending strength, $\sigma = 816 \pm 100$ MPa and Young's modulus, $E = 188 \pm 14$ GPa measured for pure zirconia may seem a little low compared to those expected for traditional yttria-stabilized zirconia. However, these values match those reported in other studies, where DLP technique was also used [21,12]. Harrer et al. investigated the influence of printing direction on the mechanical properties and obtained mean flexural strength ranging from 561 MPa to 845 MPa, for layers' orientation perpendicular and parallel to the loading direction, respectively [12]. In this study, where samples were tested perpendicularly to the loading direction, the strength is 250 MPa higher than Harrer's value, and almost reaches the 845 MPa reported for the other [12], which is surprisingly strong for the supposedly weakest orientation (i.e. layers orientation perpendicular to the loading direction).

For the sake of clarity, the mechanical properties of 3D printed alumina-zirconia ceramics of this study are reported in
Table ***2***. Moreover, previous literature results for alumina-zirconia composites fabricated by stereolithography technique are collected in Table 3, and compared to current data of AZ15 and AZ85 composites where α-alumina and 3Y-TZP are used. In the case of AZ15 we can observe that in spite the relative density was slightly lower than the values in some previous researches [43,46-48], both strength and hardness were the highest. In the case of zirconia-rich composites, current AZ85 material reached a flexural strength almost the double of that achieved by Schwarzer et al. [44], but was slightly lower than a previous reference by Borlaf et al. [45]. However, in this case, the composite was prepared at a higher alumina content (20wt%), and mechanical tests performed on machined surfaces (edges of the tensile side of the bares chamfered).

The variation of density and Young's modulus of alumina-zirconia composites shows an almost perfect linearity with the zirconia volume content, as shown in Figures 4b and 11b, further strengthening the presence of homogeneous microstructures with a good distribution of zirconia grains. Comparing the mechanical properties of the three composites, AZ15 appears to be the

best agreement to reach high hardness (H = 21 GPa) and high bending strength (σ = 693 MPa), with Young's modulus of 318 GPa and a density of 4.20 g/cm^3. Thus, mixing available alumina and zirconia slurries, in the right proportions, allows to tune the mechanical properties of alumina-zirconia composites in order to meet the required specifications for given applications.

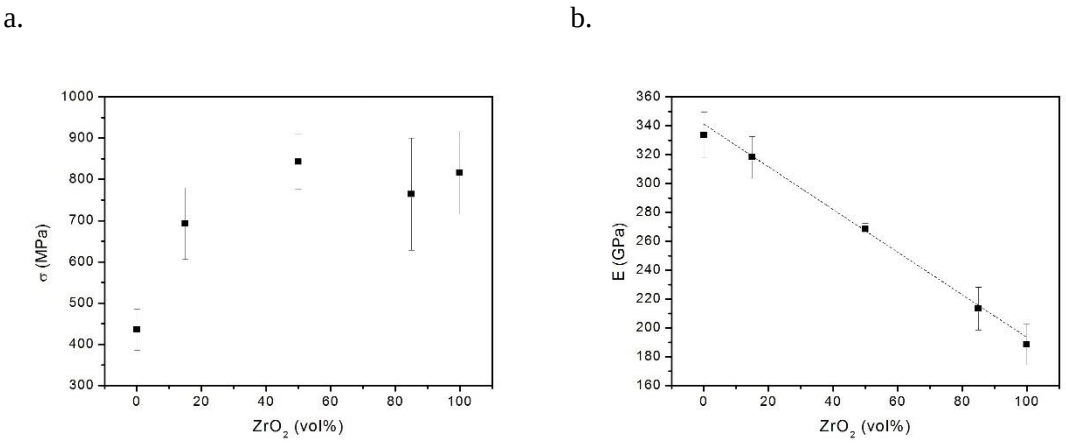

Figure 12: Variation of a. bending strength σ, and b. Young modulus E, of alumina-zirconia ceramics. Results from three point bending tests, as a function of samples composition

Table 2: Summary of mechanical properties of alumina-zirconia ceramics : ρ, density determined by Buyancy method; E, Young modulus calculated from three point bending load-displacement curve; H, hardness measured by Vickers indentation; and σ, bending strength resulting from three point bending tests

Material	A	AZ15	AZ50	AZ85	Z
Relative density (%)	98.5	98.5	98.8	99.2	99.1
H (GPa)	19.35 ± 1.08	21.14 ± 1.64	17.21 ± 0.93	15.36 ± 0.77	12.73 ± 0.25
σ (MPa)	415 ± 24	693 ±87	843 ± 67	764 ± 136	816 ± 100
E (GPa)	334 ± 16	318 ± 15	268 ± 4	213 ± 15	188 ± 14

Table 3: Literature comparison for ZTA and ATZ physical and mechanical properties

Composition	ρ (g/cm^3)	σ (MPa)	H (GPa)	Ref.
ZTA (15 vol% ZrO_2)	4.20 (98.4%)	693	21.14	This work
ZTA (15 vol% ZrO_2)	- (99.4%)	535	17.80	Xing et al. [43]
ZTA (15 vol% ZrO_2) ^	3.75 (88.5%)	-	14.10	Liu et al. [42]
ZTA (15 vol% ZrO_2) +	4.24 (99.1%)	-	17.60	Wu et al. [46]
ZTA (15 vol% ZrO_2)	4.26 (99.5%)	530	17.76	Wu et al. [48]
ZTA (20 vol% ZrO_2)	- (99.4%)	517	17.40	Zheng et al. [47]
ATZ (15 vol% Al_2O_3)	5.69 (99.2%)	764	15.36	This work
ATZ (vol% Al_2O_3 n.d.)	5.43 (98.7%)	430 °	-	Schwarzer et al. [44]
ATZ (20 vol% Al_2O_3)	5.37 (98.5%)	781 *	-	Borlaf et al. [45]

^ Sintered 1h at 1500

+ Sintered 1h at 1550

° biaxial strenght test

* Weibull flexural strength (4-point bending)

4. Conclusions

Dense alumina, zirconia and their composites were successfully fabricated by DLP-stereolithography 3D printing technology. In particular, beside neat alumina and zirconia samples, three Al_2O_3/ZrO_2 composites (containing 15, 50 and 85vol% of ZrO_2) were prepared and sintered at different temperatures in the range 1500-1600 °C. For each composite, the best sintering temperature was determined on the ground of the fired density and microstructural analysis, by determining the particle size distribution of both alumina and zirconia grains in the composites, and their evolution with the temperature. We observed a linear trend among the zirconia content and the sintered density, as well as a reverse trend between zirconia amount and

temperature required to obtain the fixed target density (ρ > 98.5%TD). In spite the easy method used to prepare composites (i.e., mixing of ready-to-print slurries), all of them showed a homogeneous microstructure with a good second-phase particles distribution in the composite materials. ZrO_2 fine grains played a key role in the microstructural refinement. In fact, in the composite at low zirconia amount (AZ15), they exerted an effective pinning on the alumina grain boundaries, thus avoiding the alumina abnormal grain growth which characterizes neat Al_2O_3 samples. In AZ50, a dual microstructure made of completely immiscible phases was produced, and here the mutual grain growth retardation was due to the longer interdiffusion distance between grains of the same phase. In AZ85, isolated alumina grains were embedded in the zirconia immiscible phase, thus making even longer the atomic diffusion distances and further preventing alumina grain growth. Once optimized the sintering conditions for the ceramic composites, mechanical properties were determined. Alumina-zirconia composites reported hardness values in the range 15-21 GPa, with an expected decrease at increasing zirconia content. Due to the fine and homogeneous microstructures, AZ15 samples reported hardness values even higher than those of neat alumina samples, while all three composites showed hardness values higher than the nominal values determined via the rule of mixtures. Very high bending strength and elastic modulus (ranging between 415-843 MPa and 188-318 GPa, respectively) were measured for all the investigated materials, being higher than the majority of the previous investigations for alumina-zirconia composites fabricated by stereolithography. The results achieved demonstrate that it is possible to avoid the long machining post-processing, while keeping high mechanical performance, strengthening this key advantage of stereolithography. Based on such promising results, more complex structures, with even more tailored microstructures will be fabricated in the future, with the aim of fully exploiting such challenging technology, and to overcome all the current limits in design and fabrication of technical ceramics.

Declaration of Competing Interest

The authors declare that they have no known competing financial interests or personal relationships that could have appeared to influence the work reported in this paper.

Acknowledgments

The researches leading to these results have received funding from the European project AMITIE (Marie Skłodowska Curie Grant Agreement n°734342).

REFERENCES

1 Ngo, T. D., Kashani, A., Imbalzano, G., Nguyen, K. T., & Hui, D. (2018). Additive manufacturing (3D printing): A review of materials, methods, applications and challenges. Composites Part B: Engineering, 143, 172-196. https://doi.org/10.1016/j.compositesb.2018.02.012

2 Coppola, B., Cappetti, N., Di Maio, L., Scarfato, P., & Incarnato, L. (2018). 3D printing of PLA/clay nanocomposites: influence of printing temperature on printed samples properties. Materials, 11(10), 1947. https://doi.org/10.3390/ma11101947

3 Liao, Y., Liu, C., Coppola, B., Barra, G., Di Maio, L., Incarnato, L., & Lafdi, K. (2019). Effect of porosity and crystallinity on 3D printed PLA properties. Polymers, 11(9), 1487. https://doi.org/10.3390/polym11091487

4 Gisario, A., Kazarian, M., Martina, F., & Mehrpouya, M. (2019). Metal additive manufacturing in the commercial aviation industry: A review. Journal of Manufacturing Systems, 53, 124-149. https://doi.org/10.1016/j.jmsy.2019.08.005

5 Gorsse, S., Hutchinson, C., Gouné, M., & Banerjee, R. (2017). Additive manufacturing of metals: a brief review of the characteristic microstructures and properties of steels, Ti-6Al-4V and high-entropy alloys. Science and Technology of advanced MaTerialS, 18(1), 584-610. https://doi.org/10.1080/14686996.2017.1361305

6 Chen, Z., Li, Z., Li, J., Liu, C., Lao, C., Fu, Y., ... & He, Y. (2019). 3D printing of ceramics: A review. Journal of the European Ceramic Society, 39(4), 661-687.

7 Zocca, A., Colombo, P., Gomes, C. M., & Günster, J. (2015). Additive manufacturing of ceramics: issues, potentialities, and opportunities. Journal of the American Ceramic Society, 98(7), 1983-2001. https://doi.org/10.1111/jace.13700

8 Galante, R., Figueiredo-Pina, C.G., Serro, A.P. Additive manufacturing of ceramics for dental applications: A review. Dental Materials, 35 (2019), pp 825-846. https://doi.org/10.1016/j.dental.2019.02.026.

9 Montanaro, L., Coppola, B., Palmero, P., & Tulliani, J. M. (2019). A review on aqueous gelcasting: A versatile and low-toxic technique to shape ceramics. Ceramics International, 45(7), 9653-9673. https://doi.org/10.1016/j.ceramint.2018.12.079

10 Deville, S. (2008). Freeze-casting of porous ceramics: a review of current achievements and issues. Advanced Engineering Materials, 10(3), 155-169. https://doi.org/10.1002/adem.200700270

11 Jabbari, M., Bulatova, R., Tok, A. I. Y., Bahl, C. R. H., Mitsoulis, E., & Hattel, J. H. (2016). Ceramic tape casting: a review of current methods and trends with emphasis on rheological behaviour and flow analysis. Materials Science and Engineering: B, 212, 39-61. https://doi.org/10.1016/j.mseb.2016.07.011

12 Harrer, W., Schwentenwein, M., Lube, T., Danzer, R. Fractography of zirconia-specimens made using additive manufacturing (LCM) technology. J Eur Ceram, 37 (2017), pp 4331-4338. https://doi.org/10.1016/j.jeurceramsoc.2017.03.018

13 Schwentenwein, M., Homa, J. Additive Manufacturing of Dense Alumina Ceramics. Int. J. Appl. Ceram. Technol., 12 (2015), pp 1-7. https://doi.org/10.1111/ijac.12319.

14 Dehurtevent, M., Robberecht, L., Thuault, A., Deveaux, E., Leriche, A., Petit, F., ... & Béhin, P. (2020). Effect of build orientation on the manufacturing process and the properties of stereolithographic dental ceramics for crown frameworks. The Journal of Prosthetic Dentistry. https://doi.org/10.1016/j.prosdent.2020.01.024

15 Johansson, E., Lidström, O., Johansson, J., Lyckfeldt, O., & Adolfsson, E. (2017). Influence of resin composition on the defect formation in alumina manufactured by stereolithography. Materials, 10(2), 138. https://doi.org/10.3390/ma10020138

16 Wu, H., Cheng, Y., Liu, W., He, R., Zhou, M., Wu, S., ... & Chen, Y. (2016). Effect of the particle size and the debinding process on the density of alumina ceramics fabricated by 3D printing based on stereolithography. Ceramics International, 42(15), 17290-17294. https://doi.org/10.1016/j.ceramint.2016.08.024

17 Shuai, X., Zeng, Y., Li, P., & Chen, J. (2020). Fabrication of fine and complex lattice structure Al 2 O 3 ceramic by digital light processing 3D printing technology. Journal of Materials Science, 1-12. https://doi.org/10.1007/s10853-020-04503-y

18 Nie, J., Li, M., Liu, W., Li, W., & Xing, Z. (2020). The role of plasticizer in optimizing the rheological behavior of ceramic pastes intended for stereolithography-based additive manufacturing. Journal of the European Ceramic Society. https://doi.org/10.1016/j.jeurceramsoc.2020.08.013

19 Zhang, K., Xie, C., Wang, G., He, R., Ding, G., Wang, M., ... & Fang, D. (2019). High solid loading, low viscosity photosensitive Al2O3 slurry for stereolithography based additive manufacturing. Ceramics International, 45(1), 203-208. https://doi.org/10.1016/j.ceramint.2018.09.152

20 Liu, W., Li, M., Nie, J., Wang, C., Li, W., & Xing, Z. (2020). Synergy of solid loading and printability of ceramic paste for optimized properties of alumina via stereolithography-based 3D printing. Journal of Materials Research and Technology, 9(5), 11476-11483. https://doi.org/10.1016/j.jmrt.2020.08.038

21 Borlaf, M., Serra-Capdevila, A., Colominas, C., & Graule, T. (2019). Development of UV-curable ZrO2 slurries for additive manufacturing (LCM-DLP) technology. Journal of the European Ceramic Society, 39(13), 3797-3803. https://doi.org/10.1016/j.jeurceramsoc.2019.05.023

22 Li, Y., Wang, M., Wu, H., He, F., Chen, Y., & Wu, S. (2019). Cure behavior of colorful ZrO2 suspensions during Digital light processing (DLP) based stereolithography process. Journal of the European Ceramic Society, 39(15), 4921-4927. https://doi.org/10.1016/j.jeurceramsoc.2019.07.035

23 Sun, J., Binner, J., & Bai, J. (2020). 3D printing of zirconia via digital light processing: optimization of the slurry and debinding process. Journal of the European Ceramic Society. https://doi.org/10.1016/j.jeurceramsoc.2020.05.079

24 He, R., Liu, W., Wu, Z., An, D., Huang, M., Wu, H., ... & Xie, Z. (2018). Fabrication of complex-shaped zirconia ceramic parts via a DLP-stereolithography-based 3D printing method. Ceramics International, 44(3), 3412-3416. https://doi.org/10.1016/j.ceramint.2017.11.135

25 Zhang, K., He, R., Xie, C., Wang, G., Ding, G., Wang, M., ... & Fang, D. (2019). Photosensitive ZrO2 suspensions for stereolithography. Ceramics International, 45(9), 12189-12195. https://doi.org/10.1016/j.ceramint.2019.03.123

26 Zhang, K., He, R., Ding, G., Feng, C., Song, W., & Fang, D. (2020). Digital light processing of 3Y-TZP strengthened ZrO2 ceramics. Materials Science and Engineering: A, 774, 138768. https://doi.org/10.1016/j.msea.2019.138768

27 Zhang, J., Wei, L., Meng, X., Yu, F., Yang, N., & Liu, S. (2020). Digital light processing-stereolithography three-dimensional printing of yttria-stabilized zirconia. Ceramics International, 46(7), 8745-8753. https://doi.org/10.1016/j.ceramint.2019.12.113

28 Masciandaro, S., Torrell, M., Leone, P., & Tarancón, A. (2019). Three-dimensional printed yttria-stabilized zirconia self-supported electrolytes for solid oxide fuel cell applications. Journal of the European Ceramic Society, 39(1), 9-16. https://doi.org/10.1016/j.jeurceramsoc.2017.11.033

29 Xing, B., Cao, C., Zhao, W., Shen, M., Wang, C., & Zhao, Z. (2020). Dense 8 mol% yttria-stabilized zirconia electrolyte by DLP stereolithography. Journal of the European Ceramic Society, 40(4), 1418-1423. https://doi.org/10.1016/j.jeurceramsoc.2019.09.045

30 Lu, Y., Mei, Z., Zhang, J., Gao, S., Yang, X., Dong, B., ... & Yu, H. (2020). Flexural strength and Weibull analysis of Y-TZP fabricated by stereolithographic additive manufacturing and subtractive manufacturing. Journal of the European Ceramic Society, 40(3), 826-834. https://doi.org/10.1016/j.jeurceramsoc.2019.10.058

31 Fu, X., Zou, B., Xing, H., Li, L., Li, Y., & Wang, X. (2019). Effect of printing strategies on forming accuracy and mechanical properties of ZrO2 parts fabricated by SLA technology. Ceramics International, 45(14), 17630-17637. https://doi.org/10.1016/j.ceramint.2019.05.328

32 Jang, K. J., Kang, J. H., Fisher, J. G., & Park, S. W. (2019). Effect of the volume fraction of zirconia suspensions on the microstructure and physical properties of products produced by additive manufacturing. Dental Materials, 35(5), e97-e106. https://doi.org/10.1016/j.dental.2019.02.001

33 Chen, F., Zhu, H., Wu, J. M., Chen, S., Cheng, L. J., Shi, Y. S., ... & Xiao, J. (2020). Preparation and biological evaluation of ZrO2 all-ceramic teeth by DLP technology. Ceramics International. https://doi.org/10.1016/j.ceramint.2020.01.152

34 Curto, H., Thuault, A., Jean, F., Violier, M., Dupont, V., Hornez, J-C., Leriche, A. Coupling additive manufacturing and microwave sintering: A fast processing route of alumina ceramics. J Eur Ceram (2019). https://doi.org/10.1016/j.jeurceramsoc.2019.11.009.

35 Zhou, M., Liu, W., Wu, H., Song, X., Chen, Y., Cheng, L., ... & Wu, S. (2016). Preparation of a defect-free alumina cutting tool via additive manufacturing based on stereolithography–Optimization of the drying and debinding processes. Ceramics International, 42(10), 11598-11602. https://doi.org/10.1016/j.ceramint.2016.04.050

36 Liu, W., Li, M., Nie, J., Wang, C., Li, W., & Xing, Z. (2020). Synergy of solid loading and printability of ceramic paste for optimized properties of alumina via stereolithography-based 3D printing. Journal of Materials Research and Technology, 9(5), 11476-11483. https://doi.org/10.1016/j.jmrt.2020.08.038

37 Zhang, K., Xie, C., Wang, G., He, R., Ding, G., Wang, M., ... & Fang, D. (2019). High solid loading, low viscosity photosensitive Al2O3 slurry for stereolithography based additive manufacturing. Ceramics International, 45(1), 203-208. https://doi.org/10.1016/j.ceramint.2018.09.152

38 Fu, X., Zou, B., Xing, H., Li, L., Li, Y., & Wang, X. (2019). Effect of printing strategies on forming accuracy and mechanical properties of ZrO2 parts fabricated by SLA technology. Ceramics International, 45(14), 17630-17637. https://doi.org/10.1016/j.ceramint.2019.05.328

39 Lu, Y., Mei, Z., Zhang, J., Gao, S., Yang, X., Dong, B., ... & Yu, H. (2020). Flexural strength and Weibull analysis of Y-TZP fabricated by stereolithographic additive manufacturing and subtractive manufacturing. Journal of the European Ceramic Society, 40(3), 826-834. https://doi.org/10.1016/j.jeurceramsoc.2019.10.058

40 Nie, J., Li, M., Liu, W., Li, W., & Xing, Z. (2020). The role of plasticizer in optimizing the rheological behavior of ceramic pastes intended for stereolithography-based additive manufacturing. Journal of the European Ceramic Society, 41(1), 646-654. https://doi.org/10.1016/j.jeurceramsoc.2020.08.013

41 Jang, K. J., Kang, J. H., Fisher, J. G., & Park, S. W. (2019). Effect of the volume fraction of zirconia suspensions on the microstructure and physical properties of products produced by additive manufacturing. Dental Materials, 35(5), e97-e106. https://doi.org/10.1016/j.dental.2019.02.001

42 Liu, X., Zou, B., Xing, H., & Huang, C. (2020). The preparation of ZrO2-Al2O3 composite ceramic by SLA-3D printing and sintering processing. Ceramics International, 46(1), 937-944. https://doi.org/10.1016/j.ceramint.2019.09.054.

43 Xing, H., Zou, B., Liu, X., Wang, X., Chen, Q., Fu, X., & Li, Y. (2020). Effect of particle size distribution on the preparation of ZTA ceramic paste applying for stereolithography 3D printing. Powder Technology, 359, 314-322. [https://doi.org/10.1016/j.powtec.2019.09.066]

44 Schwarzer, E., Holtzhausen, S., Scheithauer, U., Ortmann, C., Oberbach, T., Moritz, T., & Michaelis, A. (2019). Process development for additive manufacturing of functionally graded alumina toughened zirconia components intended for medical implant application. Journal of the European Ceramic Society, 39(2-3), 522-530. https://doi.org/10.1016/j.jeurceramsoc.2018.09.003

45 Borlaf, M., Szubra, N., Serra-Capdevila, A., Kubiak, W. W., & Graule, T. (2020). Fabrication of ZrO2 and ATZ materials via UV-LCM-DLP additive manufacturing technology. Journal of the European Ceramic Society, 40(4), 1574-1581. https://doi.org/10.1016/j.jeurceramsoc.2019.11.037

46 Wu, Z., Liu, W., Wu, H., Huang, R., He, R., Jiang, Q., ... & Wu, S. (2018). Research into the mechanical properties, sintering mechanism and microstructure evolution of Al2O3-ZrO2 composites fabricated by a stereolithography-based 3D printing method. Materials Chemistry and Physics, 207, 1-10. https://doi.org/10.1016/j.matchemphys.2017.12.021

47 Zheng, T., Wang, W., Sun, J., Liu, J., & Bai, J. (2020). Development and evaluation of Al2O3–ZrO2 composite processed by digital light 3D printing. Ceramics International, 46(7), 8682-8688. https://doi.org/10.1016/j.ceramint.2019.12.102

48 Wu, H., Liu, W., He, R., Wu, Z., Jiang, Q., Song, X., ... & Wu, S. (2017). Fabrication of dense zirconia-toughened alumina ceramics through a stereolithography-based additive manufacturing. Ceramics International, 43(1), 968-972. https://doi.org/10.1016/j.ceramint.2016.10.027

49 Wang, J., Stevens, R. Zirconia-toughened alumina (ZTA) ceramics. J Mater Sci, 24 (1989), pp 3421–3440. https://doi.org/10.1007/BF02385721.

50 Smuk, B., Szutkowska, M., & Walter, J. (2003). Alumina ceramics with partially stabilized zirconia for cutting tools. Journal of materials processing technology, 133(1-2), 195-198. https://doi.org/10.1016/S0924-0136(02)00232-7

51 Tuan, W. H., Chen, R. Z., Wang, T. C., Cheng, C. H., & Kuo, P. S. (2002). Mechanical properties of Al2O3/ZrO2 composites. Journal of the European Ceramic Society, 22(16), 2827-2833. https://doi.org/10.1016/S0955-2219(02)00043-2

52 Nevarez-Rascon, A., Aguilar-Elguezabal, A., Orrantia, E., & Bocanegra-Bernal, M. H. (2009). On the wide range of mechanical properties of ZTA and ATZ based dental ceramic composites by varying the Al2O3 and ZrO2 content. International Journal of Refractory Metals and Hard Materials, 27(6), 962-970.

53 Palmero, P., Sola, A., Naglieri, V., Belluci, D., Lombardi, M., Cannillo, V. Elaboration and mechanical characterization of multi-phase alumina-based ultra-fine composites. J Mater Sci, 47 (2012), pp 1077–1084. https://doi.org/10.1007/s10853-011-5898-5.

54 Kern, F., Palmero, P. Microstructure and mechanical properties of alumina 5vol% zirconia nanocomposites prepared by powder coating and powder mixing routes. Ceram Int, 39 (2013), pp 673-682. https://doi.org/10.1016/j.ceramint.2012.06.078.

55 Kern, F., Palmero, P., García Marro, F.G., Mestra, A. Processing of alumina–zirconia composites by surface modification route with enhanced hardness and wear resistance. Ceram Int, 41 (2015), pp 889-898. https://doi.org/10.1016/j.ceramint.2014.09.006.

56 De Aza, A. H., Chevalier, J., Fantozzi, G., Schehl, M., & Torrecillas, R. (2003). Slow-crack-growth behavior of zirconia-toughened alumina ceramics processed by different methods. Journal of the American Ceramic Society, 86(1), 115-120. https://doi.org/10.1111/j.1151-2916.2003.tb03287.x

57 https://admateceurope.com/admaflex130 (accessed 20-11-2020)

58 Quinn, G. D., Patel, P. J., Lloyd, I. Effect of Loading Rate Upon Conventional Ceramic Microindentation Hardness. Journal of research of the National Institute of Standards and Technology, 107 (2002), pp 299–306. https://doi.org/10.6028/jres.107.023.

59 MacLaren, I., Cannon, R. M., Gülgün, M. A., Voytovych, R., Popescu-Pogrion, N., Scheu, C., ... & Rühle, M. (2003). Abnormal grain growth in alumina: synergistic effects of yttria and silica. Journal of the American Ceramic Society, 86(4), 650-59. https://doi.org/10.1111/j.1151-2916.2003.tb03354.x

60 Palmero, P., Naglieri, V., Spina, G., & Lombardi, M. (2011). Microstructural design and elaboration of multiphase ultra-fine ceramics. Ceramics International, 37(1), 139-144. https://doi.org/10.1016/j.ceramint.2010.08.031

61 Kim, D. K., & Kriven, W. M. (2008). Processing and characterization of multiphase ceramic composites part I: Duplex composites formed in situ from solution. Journal of the American Ceramic Society, 91(3), 784-792. https://doi.org/10.1111/j.1551-2916.2007.01649.x

62 Garvie, R. C., & Nicholson, P. S. (1972). Phase analysis in zirconia systems. Journal of the American Ceramic Society, 55(6), 303-305. https://doi.org/10.1111/j.1151-2916.1972.tb11290.x

63 Boniecki, M., Sadowski, T., Gołębiewski, P., Węglarz, H., Piątkowska, A., Romaniec, M., ... & Łosiewicz, K. (2020). Mechanical properties of alumina/zirconia composites. Ceramics International, 46(1), 1033-1039. https://doi.org/10.1016/j.ceramint.2019.09.068

64 Kim, H. S. (2000). On the rule of mixtures for the hardness of particle reinforced composites. Materials Science and Engineering: A, 289(1-2), 30-33. https://doi.org/10.1016/S0921-5093(00)00909-6

65 Wollmershauser, J. A., Feigelson, B. N., Gorzkowski, E. P., Ellis, C. T., Goswami, R., Qadri, S. B., ... & Everett, R. K. (2014). An extended hardness limit in bulk nanoceramics. Acta Materialia, 69, 9-16. https://doi.org/10.1016/j.actamat.2014.01.030

66 Naglieri V, Palmero P, Montanaro L, Chevalier J. Elaboration of Alumina-Zirconia Composites: Role of the Zirconia Content on the Microstructure and Mechanical Properties. Materials, 6 (2013), pp 2090–2102. https://doi.org/10.3390/ma6052090. https://doi.org/10.3390/ma6052090

67 Díaz, L. A., Rivera, S., Fernández, A., Okunkova, A., Vladimirov, Y. G., Torrecillas San Millan, R. Mechanical Behavior of Alumina Toughened Zirconia Nanocomposites with Different Alumina Additions. Advances in Science and Technology, 96 (2014), pp 61–66. https://doi.org/10.4028/www.scientific.net/ast.96.61.

68 Maji, A., Choubey, G. Microstructure and Mechanical Properties of Alumina Toughened Zirconia (ATZ). Materials Today: Proceedings, 5 (2018), pp 7457-7465. https://doi.org/10.1016/j.matpr.2017.11.417.

69 Ćurković, L., Bakić, A., Kodvanj, J., & Haramina, T. (2010). Flexural strength of alumina ceramics: Weibull analysis. Transactions of FAMENA, 34(1), 13-18.

70 Dehurtevent, M., Robberecht, L., Hornez, J-C., Thuault, A., Deveaux, E., Béhin, P. Stereolithography: A new method for processing dental ceramics by additive computer-aided manufacturing. Dental Materials, 33 (2017), pp 477-485. https://doi.org/10.1016/j.dental.2017.01.018.

Figure Captions

Figure 1: FE-SEM micrographs of a) alumina and b) zirconia powder deriving from commercial slurries calcination (white arrows indicate alumina larger particles)

Figure 2: Thermal debinding cycle

Figure 3: FE-SEM micrographs (cross section) of an as-printed and water-debinded alumina sample, at lower (a) and higher (b) magnifications

Figure 4: FE-SEM micrographs of sintered alumina (1650 °C/1h) and zirconia (1500 °C/1h) printed materials

Figure 5: Density variation of alumina-zirconia composites, as a function of: a. the sintering temperature; b. the zirconia volume content at fixed temperatures (i.e. 1500 and 1550 °C)

Figure 6: FE-SEM images of AZ15 composites and related grain size distributions, as a function of sintering temperature (a. 1525, b. 1550, c. 1575 and d. 1600 °C)

Figure 7: FE-SEM images of AZ50 composites and related grain size distributions, as a function of sintering temperature (a. 1525, b. 1550, c. 1575 and d. 1600 °C)

Figure 8: FE-SEM images of AZ85 composites and related grain size distributions, as a function of sintering temperature (a. 1525, b. 1550, c. 1575 and d. 1600 °C)

Figure 9: Alumina and zirconia grain size evolution as a function of the sintering temperature for AZ15, AZ50 and AZ85 composites

Figure 10: XRD patterns corresponding to Al_2O_3, AZ15, AZ50, AZ85 and ZrO_2 samples sintered at 1625 °C, 1600 °C, 1600 °C, 1550 °C and 1500 °C for 1h, respectively. m = monoclinic ZrO_2; t = tetragonal ZrO_2 and α = α-Al_2O_3

Figure 11: Vickers hardness as a function of zirconia content. Full symbols: experimental values; empty symbols: nominal values by the rule of mixtures

Figure 12: Variation of a. bending strength σ, and b. Young modulus E, of alumina-zirconia ceramics. Results from three point bending tests, as a function of samples composition

Table Captions

Table 1: Density and mean alumina and zirconia grain size of samples submitted to mechanical testing

Table 2: Summary of mechanical properties of alumina-zirconia ceramics : ρ, density determined by Buyancy method; E, Young modulus calculated from three point bending load-displacement curve; H, hardness measured by Vickers indentation; and σ, bending strength resulting from three point bending tests

Table 3: Literature comparison for ZTA and ATZ physical and mechanical properties